Available online at www.sciencedirect.com
ScienceDirect
Acta Materialia 59 (2011) 3384–3389
Acta MATERIALIA
www.elsevier.com/locate/actamat

Comparative studies of constitutive properties of nanocrystalline and bulk iron during compressive deformation

Xiaohui Yu [a,b,c,*], Jianzhong Zhang [b], Liping Wang [d], Zejun Ding [a], Changqing Jin [c], Yusheng Zhao [b,*]

[a] Department of Physics, University of Science and Technology of China, Hefei 230026, People's Republic of China
[b] LANSCE Division, Los Alamos National Laboratory, Los Alamos, NM 87545, USA
[c] National Lab for Condensed Matter Physics, Institute of Physics, CAS, Beijing 100080, People's Republic of China
[d] Mineral Physics Institute, State University of New York, Stony Brook, NY 11794, USA

Received 8 January 2011; accepted 8 February 2011
Available online 5 March 2011

Abstract

We present a comparative study of the mechanical properties of body-centered cubic nanocrystalline iron (nano-Fe) and microcrystalline iron (micro-Fe) by in situ high-pressure synchrotron X-ray diffraction under triaxial compression. For nano-Fe with a starting high dislocation density of 10^{16} m^{-2}, the peak broadening is almost reversible upon unloading from 8.6 GPa to atmospheric pressure, indicating that no additional dislocations are built up during compressive deformation inside grains, at grain boundaries or twin boundaries. Furthermore, an orientation-dependent surface strain is found to be stored in the surface layer of the bcc nano-Fe, which is in agreement with the core–shell model of the nanocrystals. For micro-Fe, a significant and continuous peak sharpening and the associated work softening were observed after the sample is yielded at pressures above 2.0 GPa, which can be presumably attributed to a pressure-induced dislocation annihilation. This finding/interpretation supports the hypothesis that the annihilation of dislocations is one of the dominant mechanisms underlying the plastic energy dissipation. The determined yield strength of 2.0 GPa for nano-Fe is more than 15 times higher than that for micro-Fe (0.13 GPa), indicating that the nanoscale grain-size reduction is a substantially more effective strengthening mechanism than conventional carbon infusion in iron.
© 2011 Acta Materialia Inc. Published by Elsevier Ltd. All rights reserved.

Keywords: Nano iron; High pressure; Synchrotron

1. Introduction

Nanocrystalline materials, typically with grain sizes of less than 100 nm, are excellent candidates both for fundamental studies of length-scale-induced new phenomena and for novel technological applications based on atomic-level structure control via materials design [1–5]. Over the last decade, extensive efforts, both experimental (Cu [6,7], Al [8], Ni [9,10]) and theoretical [11,12], have been devoted to revealing and understanding the deformation mechanisms of nanocrystalline materials. It has been suggested that at a critical grain size, 20–40 nm for face-centered cubic (fcc) metals, grain boundary sliding and migration become the dominant deformation mechanisms because the stress to bow out dislocations approaches the theoretical shear stress. However, most previous investigations were conducted using conventional uniaxial tensile methods on fcc nanocrystalline metals and on a limited number of dense specimens with necking where the deformation cannot drive the intrinsic mechanical behavior and plastic deformation mechanisms in nanocrystalline materials. Few deformation experiments, on the other

* Corresponding authors. Address: LANSCE Division, Los Alamos National Laboratory, Los Alamos, NM 87545, USA (X. Yu). Tel.: +1 505 948 6546; fax: +1 505 665 2676.
E-mail addresses: xiaohui@lanl.gov (X. Yu), yzhao@lanl.gov (Y. Zhao).

1359-6454/$36.00 © 2011 Acta Materialia Inc. Published by Elsevier Ltd. All rights reserved.
doi:10.1016/j.actamat.2011.02.013

hand, have been conducted in triaxial compression mode, particularly on body-centered cubic (bcc) metals. Furthermore, some recent studies have revealed that grain boundaries [13–15] and twin boundaries [16] can act as dislocation nucleation sites and hence govern the strength of fcc materials; however, it is not known whether this will happen in bcc metals. To fully understand the properties of nanocrystalline metals during deformation, especially the dislocation behavior, we have conducted triaxial high-pressure compression deformation experiments on both microcrystalline and nanocrystalline Fe using in situ synchrotron X-ray diffraction with peak width analysis. The two Fe samples were studied in a single high-pressure experiment to allow direct and accurate comparison of properties between the pair of samples.

2. Experimental methods

The microcrystalline iron (micro-Fe, from Alfa Aesar) used is 99.9% pure and has a grain size distribution of 3–10 μm. This micro-Fe was also used as the starting material for preparation of nanocrystalline iron (nano-Fe) using a high-energy ball milling technique [17]. Micro-Fe powders (5–8 g) were ball-milled for 30 h using a SPEX 8000 mill, hardened steel vials and 30 1 g hardened steel balls. The SEPX mill was operated inside an argon-filled glovebox containing less than 1 ppm oxygen, so that any contaminant was Fe from the steel ball and vial. In Ref. [17], we also calculated the dislocation density in nano-Fe based on neutron diffraction peak profile analysis. This analysis shows that a great quantity of dislocations, with a density of 10^{16} cm^{-2}, are generated and stored inside the particles during the ball-milling process. The starting nano-Fe has a bcc crystal structure and an average grain size of 12 nm, derived from the peak profile analysis of diffraction data. The in situ X-ray diffraction experiment was performed using a cubic-anvil apparatus installed on beamline X17B2 of the National Synchrotron Light Source (NSLS), Brookhaven National Laboratory [18]. The white radiation from the superconducting wiggler magnet was used for energy-dispersive measurements. The diffracted X-rays were collected with a multi-element detector at a fixed Bragg angle of $2\theta = 6.69°$. The nano-Fe and micro-Fe samples, sandwiched by NaCl powders, were packed into a solid pressure medium made of a mixture of amorphous boron and epoxy resin. NaCl was also used as an internal pressure marker and the sample pressure was calculated from Decker's equation of state for NaCl [19]. At each experimental condition, five NaCl diffraction peaks, 111, 200, 220, 222 and 420, were usually used to determine the pressure. Within the accuracy of the Decker scale for NaCl, the uncertainty in pressure measurements is mainly due to the statistical variation in the positions of different diffraction peaks and is less than 0.2 GPa in the pressure range of this study.

The two Fe samples were compressed at room temperature up to 8.6 GPa, with X-ray diffraction data collected at steps of 0.3–0.5 GPa during compression and at steps of ~0.5 GPa during decompression. A counting time of ~1 min is typically used for each diffraction pattern. Examples of X-ray diffraction patterns at selected conditions are shown in Fig. 1; no phase transition to an hexagonal close-packed phase was observed in the experimental pressure range.

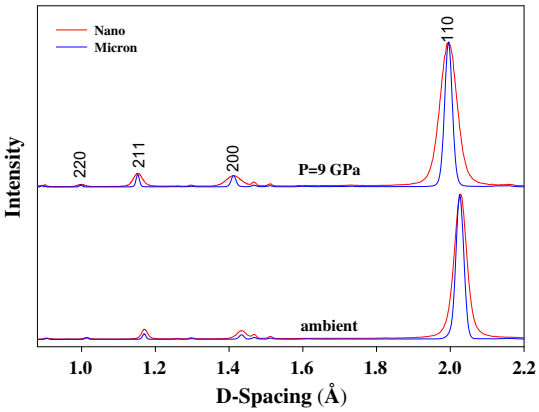

Fig. 1. Representative X-ray diffraction patterns for nano-Fe (red) and micro-Fe (blue) at different pressure conditions. The significant peak broadening of nano-Fe was observed as severe differential stresses built up on the crystal grains at high pressure. The peak intensities of the *hkl* diffractions are normalized for width comparison. Some minor peaks in the patterns are lead (Pb) fluorescence peaks, which do not change with *P–T* conditions. (For interpretation of the references to color in this figure legend, the reader is referred to the web version of this article.)

The stress and strength of nano- and micro-Fe were derived from peak profile analysis. The detailed method was outlined by Weidner et al. [20] and recently modified by Zhao and Zhang [20,21]. Generally speaking, the polycrystalline diffraction profile is a convolution function of instrument response, grain size distribution and crystal lattice deformations along the diffraction vector. During high-pressure compression experiments, the amount of peak broadening indicates the distribution of deviatoric stress along the diffraction vector, which is typically due to different crystalline orientations relative to the loading direction, and particularly to the stress concentration at grain-to-grain contacts during the powder compaction [20–22]. The diffraction peak widths reach the maximum as the deviatoric stress approaches the ultimate yield strength and the sample material begins to flow plastically. By monitoring the peak width variation of different *hkl* diffractions as a function of pressure, one can derive the differential strain, and thus the yield strength of the sample materials.

3. Results and discussion

Following our previous work [21–23], we express the full width at half maximum (FWHM) of diffraction peaks in ångströms as Δd (FWHM). To facilitate peak width comparison between nano- and micro-Fe, we set the initial (i.e. ambient pressure) peak width of different *hkl* at zero, and then normalize these relative to the corresponding

maximum values observed; therefore, the normalized FWHM is expressed as $(\Delta d - \Delta d_{\text{initial}})/(\Delta d_{max} - \Delta d_{\text{initial}})$. Inspection of Fig. 2 indicates that the peak width variation of nano-Fe during pressure loading and unloading is substantially different from that of micro-Fe. For nano-Fe (Fig. 2a), the diffraction peaks broaden linearly with pressure up to ~2.0 GPa, corresponding to the regime of elastic deformation, and then at higher pressures deviate from linearity before reaching a plateau. Upon unloading, diffraction peaks are almost recovered to their original width, a finding that is different to our previous results on fcc nano-Ni obtained using the same experimental tequnique [22], which shows a 84% recovery in peak width.

An increasing dislocation density in coarse-grained metals has been considered as one of the main contributing factors behind the peak broadening [24]. Normally, for microscale materials, the dislocations move and interact with each other easily and also create new dislocations when plastic deformation begins. A macroscopic manifestation of these processes, as experimentally demonstrated in coarse-grained metals such as Cu [9] and Ni [23], is an irreversible peak width broadening (up to 50%) in unloaded samples relative to the undeformed states, a phenomenon that is generally attributed to the accumulation of a residual dislocation network during the plastic deformation [9]. Following this line of reasoning, the striking feature of an almost 100% peak width recovery in bcc nano-Fe after unloading not only suggests that the dislocations are fixed inside the grains but also infers that no additional dislocations are generated during the plastic deformation. This conclusion is consistent with atomistic computer simulations [11] in the sense that there exists a critical length scale, typically less than 20–40 nm in fcc metals, below which a dislocation source can no longer propagate and interact with pre-existing structures or with each other. In addition, a similar conclusion was drawn based on the reversible peak broadening observed during the deformation of fcc nano-Ni [9]. By the same token, the dislocation nucleation at the grain and twin boundaries, as observed in fcc nanocrystalline materials [13–16], does not seem to happen in our bcc nano-Fe samples. All these observations support the common belief that the mechanical property of nanocrystalline metals is primarily mediated by grain boundary behavior such as sliding and rotating.

For micro-Fe (Fig. 2b), the diffraction peaks broaden linearly with increasing pressure up to ~1.7 GPa. Upon further compression, we observed continuous peak sharpening with increasing pressure. At the highest pressure of the experiment (~8.6 GPa), the (1 1 0) peak width is even sharper than its initial value. This behavior is peculiar because it has thus far not been observed in other metals [22] or in ceramic materials [23]. It is well recognized that the diffraction peak width is primarily determined by three main factors: (i) instrument contribution, (ii) crystallite size effect and (iii) inhomogeneous strain. It is also well known that the crystallite size effects on the diffraction peak width, as described by the Scherrer equation, are limited to nanoscale particles and cannot be applied to micron-sized crystal grains. As a result, the presence/absence of grain growth has no effect on the observed peak width in micron-Fe. Because of this, and also because dislocation is one of major contributors to the inhomogeneous strain, we attribute this phenomenon to a pressure-induced dislocation annihilation, which will be further discussed later in this paper.

The FWHMs of the diffraction peaks can be used to quantify the differential strain, ε, introduced by stress heterogeneity, lattice deformation and dislocation density at high pressure. The FWHMs can also be used to quantify the contributions of instrument response (Δd_{ins}) and grain sizes (Δd_{size}), in the form of [21,22]:

$$\Delta d_{obs}^2/d^2(P) = (\varepsilon^2 + \Delta d_{ins}^2/d^2) + (\kappa/L)^2 g d^2(P), \quad (1)$$

where Δd_{obs} and Δd_{ins} are the observed peak width and the peak width at a stress/dislocation-free state, respectively, d

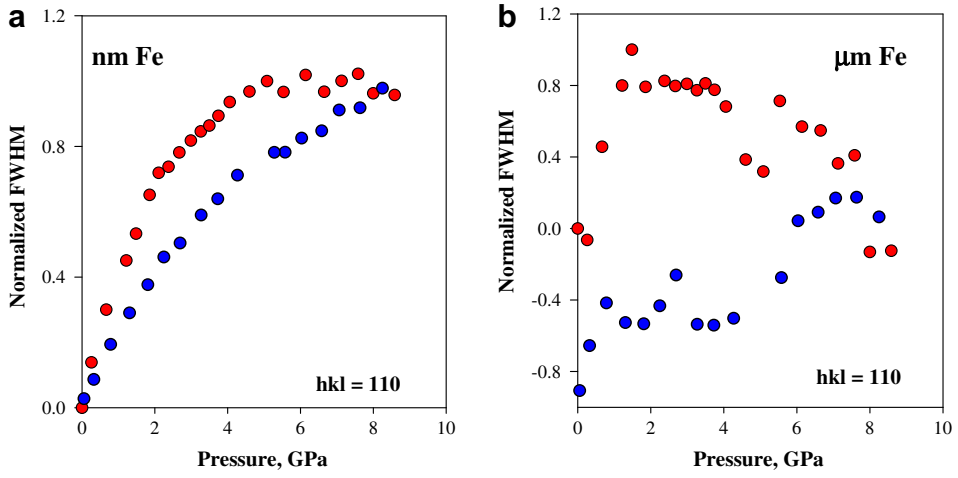

Fig. 2. Peak width vs. pressure for nano-Fe (a) and micro-Fe (b). The red circles are for the pressure loading process and the blue circles indicate the unloading process. (For interpretation of the references to color in this figure legend, the reader is referred to the web version of this article.)

is the d-spacing of a given lattice plane, and L the material's grain size, obtained via the Scherrer equation [25]. Note that Eq. (1) is essentially equivalent to the classic Williamson–Hall (W–H) method and its subsequent variations. With the FWHM expressed in ångströms, Eq. (1) can be applied to any diffraction data, independent of detection mode (energy dispersive, angular dispersive and time-of-flight). Eq. (1) is a typical $Y = a + b \cdot X$ plot. Therefore, one can derive the apparent strain, $\varepsilon^2_{apparent} = (\varepsilon^2 + \Delta d^2_{ins}/d^2)$, and the average grain size, L, from the ordinate intercept and the slope of the $\Delta d^2_{obs}/d^2$ vs. $d^2(P)$ plot, respectively. Examples of such derivation from diffraction data at ambient conditions are illustrated in Fig. 3. For the micro-Fe sample (Fig. 3, right panel), all the raw data line up quite nicely; however, for the nano-Fe sample (Fig. 3, left panel), the raw data are highly scattered, which was also observed in nanocrystalline Ni in our previous work [22]. The observed data scattering can be understood in terms of the so-called core–shell model [26–28], which views a nanocrystal as two structurally distinct components, a crystalline component formed by small single crystal and a surface layer characterized by a significant fraction of atoms at grain boundaries. The interatomic distance in the surface layer typically differs (reduced or expanded) from that in a perfect crystal lattice, leading to internal strains within the surface atoms. This surface/internal strain is crystal-orientation dependent, and is responsible for the scattering on the $\Delta d^2_{obs}/d^2$ vs. $d^2(P)$ plot. In recent years, Ungar and co-workers have proposed a different approach to account for diffraction peak broadening as a result of line defects [24,29,30]. In this approach, dislocations are assumed to be the main contributors to the residual strain and, correspondingly, the scatter in the so-called W–H plot (note that our Fig. 3 is a modified W–H plot) is attributed to the anisotropy of the dislocation strain field.Due to concerns over the surface/internal strain, we had previously induced a diffraction elasticity ratio, DER, to correct this strain anisotropy [22]. For nano-Fe, DER $= (E_{hkl}/E_{110})$, where E_{hkl} is the Young's modulus for different hkl lattice planes and E_{110} is the least compliant plane chosen as a reference. By scaling DER^2 to the observed raw data, we correct the strain differences on the individual lattice planes. The corrected data, as illustrated in Fig. 3 (left panel), can be readily fit to a straight line in the $\Delta d^2_{obs}/d^2$ vs. $d^2(P)$ plot and allow us to derive unambiguously the apparent strain and grain size information. The DER^2 correction for bcc nano-Fe, along with our previous results on fcc nano-Ni [22], indicates that the surface/internal strain is not only stored in the shell area of the nanograins but is also crystal-orientation dependent, and therefore provides another line of evidence that supports the core–shell model for a nanocrystal.

The apparent strains derived using Eq. (1) can be converted to the apparent stress through $\sigma_{app} = E\varepsilon_{app}$, where E is the Young's modulus of Fe. In this work, we assume that nano- and micro-Fe have the same value of E, 211 GPa. The apparent stresses are plotted as a function of pressure in Fig. 4. The initial difference between nano-Fe and micro-Fe is due to residual stress, surface strain and grain size effects. As pressure increases, the grain-to-grain contact stresses enhance at a much greater rate in nano-Fe during the elastic–plastic transition region. In Fig. 4 (left panel), we observe an obvious yield (kink) point for nano-Fe at $P = 2.1$ GPa, corresponding to a yield strength of $\Delta\sigma^{nm}_{yield} = 2.0$ GPa. In micro-Fe (Fig 4, right panel), the yield point is located at $P = 1.7$ GPa with $\Delta\sigma^{\mu m}_{yield} = 0.13$ GPa, which is in good agreement with the literature value [31]. The observed 15-fold strengthening in nano-Fe is consistent with the classic Hall–Petch law [32,33], which indicates a significant increase in the strength of the polycrystals as grain size decreases, though a totally different mechanism in involved here. For micro-Fe, the plastic deformation is mediated by dislocation behavior. Therefore, through the infusion of C atoms (or other impurities) into Fe, one can stop the movement of the dislocations and subsequently strengthen Fe, and obtain a yield

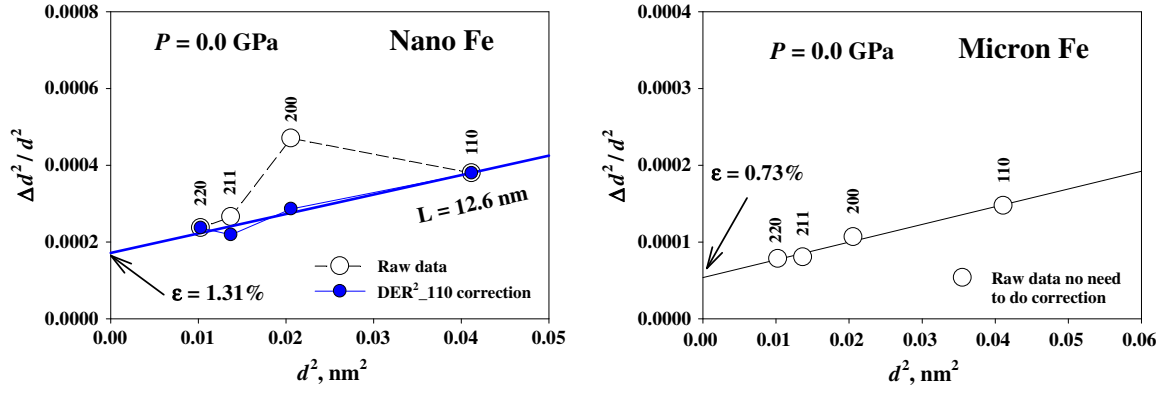

Fig. 3. The plot of $\Delta d^2_{obs}/d^2$ vs. $d^2(P)$ according to Eq. (1) at ambient conditions. (Left) The highly scattered raw data of nano-Fe are shown as the open black circles and the data corrected by DER$^2 = (E_{hkl}/E_{110})^2$ are shown as solid blue symbols. The linear regression results of the DER^2-corrected data are shown by the straight lines; the ordinate intercepts provide apparent strains and the plot slopes provide grain size information. (Right) The raw data for micro-Fe sample. It is clear that all the raw data line up quite nicely and no DER^2 corrections are needed.

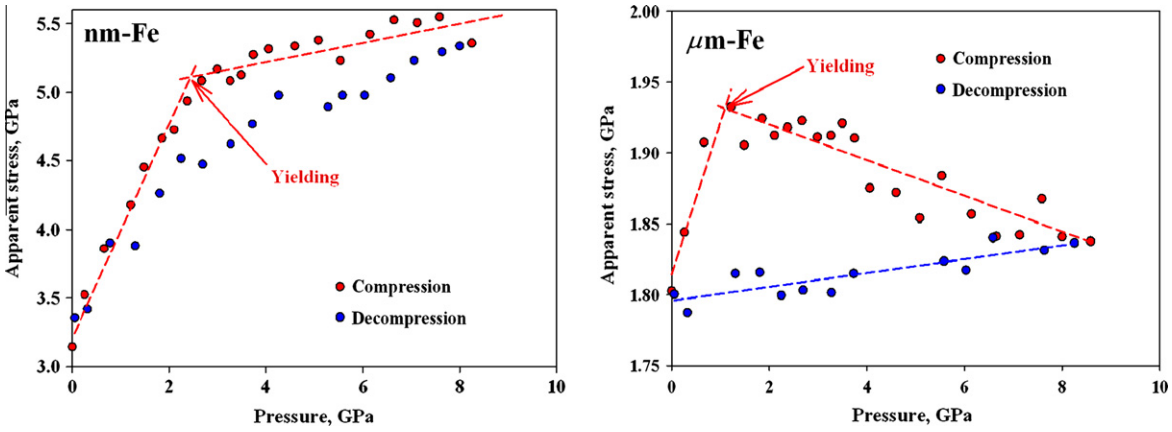

Fig. 4. Apparent stresses of nano-Fe and micro-Fe plotted as a function of pressure, which includes both microstrain and instrument-zero effects. The "yielding" points are derived from the intersections of elastic loading and plastic work-hardening/softening stages.

strength of ~0.6 GPa (for steel). However, in nano-Fe, the plastic deformation is mediated by grain boundary behaviors, and the dislocations seem to be frozen inside the grains such that the strength (2.0 GPa) becomes substantially higher than that of steel. Furthermore, nano-Fe exhibits a significant work hardening after yield, whereas in micro-Fe, there is continuous work softening at pressures above 1.7 GPa.

It is well known that plastic deformation in coarse-grained metals is controlled by dislocation-mediated processes. For materials whose flow stress is governed directly or indirectly by dislocation interactions during plastic stage, the Taylor relationship predicts the flow stress of a slip system to be proportional to the square root of dislocation density ρ:

$$\sigma = \sigma_0 + K\rho^{1/2},$$

where K is a constant. It is also recognized that the diffraction peak width of coarse-grained materials is proportional to dislocation density during plastic deformation. The fact that micro-Fe shows continuous peak sharpening and work softening in the plastic stage indicates that dislocations partially annihilate as a result of propagation and interaction, which in turn leads to the decrease in dislocation density. Because dislocation interaction would also result in generation of new dislocations, it can be inferred that annihilation dominates the dislocation-mediated processes during compressive deformation of micro-Fe. In metals, the plastic deformation during tensile tests is typically irreversible and also leads to the work hardening and increase in dislocation density. The present findings on micro-Fe represent entirely new phenomena associated with dislocation-mediated processes, either due to the pressure effect and/or the distinction between tensile and compressive modes of deformation.

Energy dissipation during plastic deformation is another important aspect of the mechanical properties of metals. It is generally accepted that most of the externally applied mechanical energy during plastic deformation is dissipated as heat, with only a small proportion stored in the crystal lattice as strain energy. The exact mechanisms by which the mechanical energy is dissipated, however, have still not been well understood. Although a number of hypotheses have been proposed [34], the subsequent debate has focused on the roles of creation and annihilation of point defects [34] and dislocations [35,36] during plastic deformation. To take our discussion in the preceding paragraph one step further, our findings seem to be consistent with the hypothesis that the annihilation of dislocations is the dominant dissipative mechanism, and therefore sheds some light on the plastic energy dissipation. In addition, as illustrated in Fig. 2, the dissipation loop (i.e. loading–unloading hysteresis loop) for micro-Fe is much larger than that for nano-Fe, indicating an enhanced energy loss during plastic deformation of micro-Fe. It can be hypothesized that this enhanced level of energy dissipation provides a sufficient driving force for dislocation annihilation to occur.

4. Conclusions

In summary, we carried out a comparative study between nanocrystalline and microscale bcc Fe under the triaxial compression and determined their constitutive properties from diffraction peak profile analysis. We observed a reversible peak broadening in nano-Fe during loading/unloading, indicating that the plastic deformation in nano-Fe, even with a starting high dislocation density of 10^{16} m^{-2}, is no longer governed by dislocation-mediated processes. Furthermore, an orientation-dependent surface strain is found to be stored in the surface layer of the bcc nano-Fe, which is in agreement with the core–shell model of the nanocrystals. For micro-Fe, a significant and continuous peak sharpening and the associated work softening were observed after the sample yields, a peculiar finding that can presumably be attributed to pressure-induced dislocation annihilation. This finding/interpretation supports the hypothesis that the dislocation annihilation is one of

the dominant mechanisms underlying plastic energy dissipation. Our results also show that the yield strength of nano-Fe is 15 times larger than that of micro-Fe and more than 3 times higher than that of carbon-infused iron (steel), indicating that grain-size reduction is more effective route for strengthening iron.

Acknowledgments

This research is supported by Los Alamos National Laboratory, which is operated by Los Alamos National Security LLC under DOE Contract DE-AC52-06NA25396. The experimental work was carried out at beamline X17B2 at the National Synchrotron Light Source, Brookhaven National Laboratory, which is supported by the Consortium for Materials Properties Research in Earth Sciences (COMPRES) under NSF Cooperative Agreement EAR 01-35554.

References

[1] Gleiter H. Prog Mater Sci 1989;33:223.
[2] Goldstein AN, Echer CM, Alivisatos AP. Science 1992;256:1425.
[3] Chen C, Herhold AB, Johnson CS, Alivisatos AP. Science 1997;276:398.
[4] Buuren TV, Dinh LN, Chase LL, Siekhaus WJ, Terminello LJ. Phys Rev Lett 1998;80:3803.
[5] Champion Y, Langlois C, Guerin-Mailly S, Langlois P, Bonnentien J, Hytch MJ. Science 2003;300:310.
[6] Liao XZ, Zhao YH, Srinivasan SG, Zhua YT, Valiev RZ, Gunderov DV. App Phys Lett 2004;84:592.
[7] Lu L, Chen X, Huang X, Lu K. Science 2009;323:607.
[8] Chen M, Ma E, Hemker KJ, Sheng H, Wang Y, Cheng X. Science 2003;300:127523.
[9] Budrovic Z, Swygenhoven HV, Derlet PM, Petegem SV, Schmitt B. Science 2004;304:273.
[10] Shan Z, Stach EA, Wiezorek JMK, Knapp JA, Follstaedt DM, Mao SX. Science 2004;305:654.
[11] Swygenhoven HV. Science 2002;296:66.
[12] Schiotz J, Jacobsen KW. Science 2003;301:1357.
[13] Espinosa HD, Berbenni S, Panico M, Schwarz KW. PNAS 2005;102:16933.
[14] Bobylev SV, Ovidko IA. Phys Solid State 2008;50:642.
[15] Yamakov V, Wolf D, Phillpot SR, Mukherjee AK, Gleiter H. Nat Mater 2004;3:43.
[16] Li X, Wei Y, Lu L, Lu K, Gao H. Nature 2010;464:877.
[17] Shen TD, Schwarz RB, Feng S, Swadener JG, Huang JY, Tang M, et al. Acta Mater 2007;55:5007.
[18] Weidner DJ, Vaughan MT, Wang J, Liu X, Pacalo RE, Zhao Y. In: Syono Y, Manghnani MH, editors. High-pressure research: application to earth and planetary sciences. Washington (DC): American Geophysics Union; 1992. p. 13.
[19] Decker DL. J Appl Phys 1971;42:3239.
[20] Weidner DJ, Wang Y, Vaughan MT. Science 1994;266:419.
[21] Zhao Y, Zhang J. J Appl Crystallogr 2008;41:1095.
[22] Zhao Y, Zhang J, Clausen B, Shen TD, Gray GT, Wang L. Nano Lett 2007;7:426.
[23] Wang Y, Zhang J, Zhao Y. Nano Lett 2007;7:3196.
[24] Ungar T, Gubicza J, Ribarik G, Borbely A. J Appl Crystallogr 2001;34:298.
[25] Simmons G, Wang H. Single crystal elastic constants. Cambridge (MA): MIT Press; 1997.
[26] Gleiter H. Prog Mater Sci 1989;33:223.
[27] Palosz B, Stelmakh S, Grzanka E, Gierlotka S, Pielaszek R, Bismayer U, et al. J Phys: Condens Mater 2004;16:s353.
[28] Zhang J, Zhao Y. Appl Phys Lett 2007;90:043112.
[29] Revesz A, Ungar T, Borbely A, Lendvai J. Nanostruct Mater 1996;7:779.
[30] Ungar T, Tichy G. Phys Status Solidi A 1999;171:425.
[31] Okada A, Maeda H, Hamada K, Ishida I. J Nucl Mater 1999;271:133.
[32] Hall EO. Proc Phys Soc Lond, Ser B 1951;64:747.
[33] Petch NJ. J Iron Steel Inst 1953;174:25.
[34] Nicholas JF. Acta Metall 1959;7:544.
[35] Nakada Y. Philos Mag 1965;11:251.
[36] Plekhov OA, Saintier N, Naimark O. Tech Phys 2007;52:1236.